



A Comparative Study of CoNi-LDH/ZnO Film for Photocathodic Protection Applications in the Marine Environment

Xuan Zhang¹, Yanhua Wang^{1*}, Dongmei Zhang¹ and Zhencheng Tao^{2,3,4*}

¹Key Laboratory of Marine Chemistry Theory and Technology, College of Chemistry and Chemical Engineering, Ministry of Education, Ocean University of China, Qingdao, China, ²Key Laboratory of Marine Ecology and Environmental Sciences, Institute of Oceanology, Chinese Academy of Sciences, Qingdao, China, ³Laboratory for Marine Ecology and Environmental Science, Qingdao National Laboratory for Marine Science and Technology, Qingdao, China, ⁴Center for Ocean Mega-Science, Chinese Academy of Sciences, Qingdao, China

OPEN ACCESS

Edited by:

Changdong Gu,
Zhejiang University, China

Reviewed by:

Ahmed Abdel Nazeer,
Kuwait University, Kuwait
Fahe Cao,
Sun Yat-sen University, China
Ghulam Yasin,
Beijing University of Chemical
Technology, China

*Correspondence:

Zhencheng Tao
taozc@qdio.ac.cn
Yanhua Wang
wyhazz@163.com

Specialty section:

This article was submitted to
Environmental Degradation of
Materials,
a section of the journal
Frontiers in Materials

Received: 25 March 2022

Accepted: 19 April 2022

Published: 03 June 2022

Citation:

Zhang X, Wang Y, Zhang D and Tao Z
(2022) A Comparative Study of CoNi-
LDH/ZnO Film for Photocathodic
Protection Applications in the
Marine Environment.
Front. Mater. 9:904555.
doi: 10.3389/fmats.2022.904555

In this study, two kinds of Co–Ni-layer double hydroxide (LDH)/ZnO films were prepared with different morphologies by a simple electrochemical method. The properties of the films were investigated by SEM, XRD, UV–Vis DRS, XPS, and electrochemical techniques. It was found that Co–Ni-LDH-modified ZnO films exhibited excellent photocathodic properties in a scavenger-free environment. This is mainly due to the absorption of visible light by LDH, the formation of *p–n* heterojunction, and the depletion of photo-generated holes by the cycling process of Co (II)/Co (III). Compared with CoNi-LDH/ZnO nanorods, CoNi-LDH/ZnO nanoclusters showed better photocathodic protection performance and physical barrier effect. Under illumination conditions, the rough surface of ZnO nanoclusters and the deposition of a large amount of LDH can provide more photoelectrochemical active sites, thus improving the light absorption capacity and photocathodic protection performance of CoNi-LDH/ZnO nanoclusters. Under dark conditions, the physical barrier effect of CoNi-LDH/ZnO nanoclusters was also enhanced by the dense ZnO nanoclusters and thick CoNi-LDH layers.

Keywords: photocathodic protection, CoNi-LDH, ZnO nanocluster, 304 stainless steel, electrochemical method

INTRODUCTION

Photocathodic protection is one of the most promising anticorrosion technologies, which has attracted widespread attention in recent years (Bu and Ao, 2017; Xu et al., 2021). This technology can protect the connected metal by injecting the photo-generated electrons into the metal and shifting the potential negatively, which requires no applied current and very little consumption of the photoanode material (Yuan and Tsujikawa, 1995). At present, a variety of semiconductor nanomaterials (Xuan et al., 2018; Yang and Cheng, 2018; Bai et al., 2019; Ding et al., 2019; Qiu et al., 2019; Liu et al., 2020; Lu et al., 2020; Jing et al., 2021) have been applied as the photoanode materials, such as TiO₂, G-C₃N₄, BiVO₄, and ZnO. According to the published work (Bu and Ao, 2017; Xu et al., 2021), most photoanodes show good photoelectrochemical performance in solutions containing hole scavengers but are not suitable for actual seawater environments. In order to realize the practical application of photocathodic protection technology, it is necessary to develop photoanode materials suitable for the marine environment.

ZnO has been commonly adopted due to its high photocatalytic activity (Kang et al., 2019; Xu et al., 2021) and suitability for seawater applications (Li et al., 2018; Li et al., 2019; Liu et al., 2020). ZnO is an n-type semiconductor with controllable microstructure, which can form a variety of nanostructures, including nanorods (He and Wang, 2011; Yang and Cheng, 2018; Wei et al., 2020), nanowires (Lin and Liu, 2021), and nanoparticles (Sun et al., 2014). The morphology of ZnO has a great influence on its photocathodic protection performance (Liu et al., 2021), which can be regulated by the deposition temperature, material concentration, current density, etc (Jabbar et al., 2017; Yasin et al., 2018a; Yasin et al., 2018b).

Despite this, as a photoanode, ZnO has a large band gap and can only absorb ultraviolet light; thus, its utilization efficiency of sunlight is very low. In addition, the rapid recombination of photo-generated carriers is another problem to be considered. To solve these problems, modification of ZnO with other semiconductor materials is a feasible way to improve its photoelectric properties in practical applications (Xu et al., 2014; Jing et al., 2015; Yang et al., 2019; Wei et al., 2020).

As one kind of hydroxide-like material (Cao et al., 2022), layered double hydroxides (LDHs) are used as barriers against corrosive media due to their excellent physical barrier and trapping ability of corrosive ions (Guo et al., 2019; Tabish et al., 2021; Zhou et al., 2021). Some LDHs were also used as semiconductor materials owing to their excellent absorption capacity for visible light (Guo et al., 2019; Zhou et al., 2021). In particular, LDHs containing transition metal elements, such as Co, Ni, or Fe, have a good performance in the field of photo-electrochemical water-splitting due to their high specific surface area, short photo-carrier transmission path, and low-cost (Shao et al., 2014; Wang G. et al., 2018; Zhu et al., 2018). The ZnO@CoNi-LDH nanowire was prepared by the hydrothermal synthesis method, and the nanowire array exhibited excellent photo-electrochemical water oxidation activity (Shao et al., 2014). Not only in the field of water-splitting, LDHs also played an important part in the photocathodic protection field. ZnFeAl-LDHs modified by TiO₂ had superior photocathodic protection performance under visible light (Wang X.-T. et al., 2018). A layer of NiGa-LDH was prepared on TiO₂ by the hydrothermal method, and the formation of heterojunction improved the photocathodic protection performance during the long-term test (Chen et al., 2021). Some researchers prepared α -Fe₂O₃ photoanode modified by NiFe(OH)_x and confirmed that the LDH materials could capture holes and enhance the photocathodic protection performance (Fan et al., 2020). In addition, LDHs have excellent physical barrier effect and hydrophobicity, which can inhibit the entry of aggressive ions and protect the underlying metal substrate under dark conditions (Tedim et al., 2016). For example, the NiAl-LDH film was covered on the surface of 304SS by the electrodeposition method, and the LDH film exhibited excellent protective properties under dark and light conditions (Zhou et al., 2021).

In this work, considering the excellent physical barrier and photo-electrochemical properties of LDHs, two kinds of CoNi-LDH/ZnO films were prepared by a simple and rapid electrochemical method. Then, the properties of the films were

characterized, the photocathodic protection performances were measured, and the anticorrosion mechanism was discussed.

EXPERIMENTAL DETAILS

Preparation of the ZnO Film

The 304SS specimens were connected with copper wires and sealed with epoxy resin, leaving the exposure area of $1 \times 1 \text{ cm}^2$. Then, they were polished with 2000 grit SiC papers and cleaned with ethanol and water, successively. ZnO nanoclusters (ZnO-C) were prepared on 304SS by a facile electrochemical method. A three-electrode system was used, and 304SS, platinum foil, and saturated calomel electrode (SCE) were selected as the working electrode (WE), the counter electrode (CE), and the reference electrode (RE), respectively. Electrodeposition was carried out in 5 mM Zn(NO₃)₂ solution in the potentiostatic mode for 1 h with a potential of -1.0 V (vs. SCE). The temperature of the electrolyte was maintained at 40°C to obtain ZnO-C. The ZnO nanorod (ZnO-R) was prepared according to the previous literature (Liu et al., 2021), and the electrodeposition temperature was maintained at 60°C.

Preparation of CoNi-LDH/ZnO Film

The 304SS electrodes covered with the ZnO film (ZnO-C or ZnO-R) were used as the working electrode to deposit the CoNi-LDH/ZnO film in the mixed solution of 20 mM Co(NO₃)₂ and 10 mM Ni(NO₃)₂. The electrodeposition was operated at -1.0 V (vs. SCE) for 300 s to obtain the LDH/ZnO-C, while the LDH/ZnO-R was prepared by the method according to the previous literature with a deposition time of 60 s (Shao et al., 2014). Afterward, the samples were rinsed with deionized water and dried for 12 h (60°C).

Characterization

The microstructure of the samples was analyzed by scanning electron microscopy (SEM, ZEISS Gemini Sigma 300). Elemental analysis was investigated by the energy-dispersive spectroscopy (EDS). X-ray diffraction (XRD, Rigaku Ultima IV) in Bragg-Brentano configuration with Cu-K α radiation was used for phase identification. UV-Visible diffuse reflectance spectra (UV-DRS) of the samples were recorded by using a UV-Vis spectrophotometer (Hitachi U-3900H) with an integrating sphere attachment to evaluate the photo absorption performance of the samples.

Photoelectrochemical and Electrochemical Measurements

An electrochemical workstation (CHI660E, Shanghai Chenhua Instrument Co. Ltd., China) was used to investigate the photoelectrochemical (PEC) performance of the prepared samples. The modified 304SS electrode, Pt electrode, and saturated calomel electrode (SCE) were used as WE, CE, and RE, respectively. All electrodes were tested in 3.5 wt% NaCl solution using cylindrical quartz beakers as containers. The open-circuit potential (OCP) was recorded under intermittent

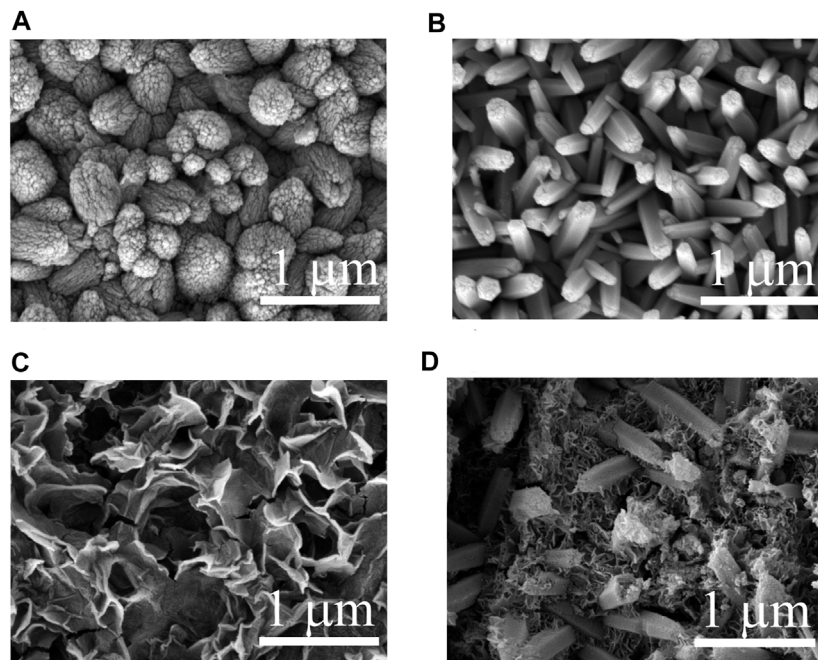


FIGURE 1 | SEM images of ZnO-C (A), ZnO-R (B), LDH/ZnO-C (C), and LDH/ZnO-R (D).

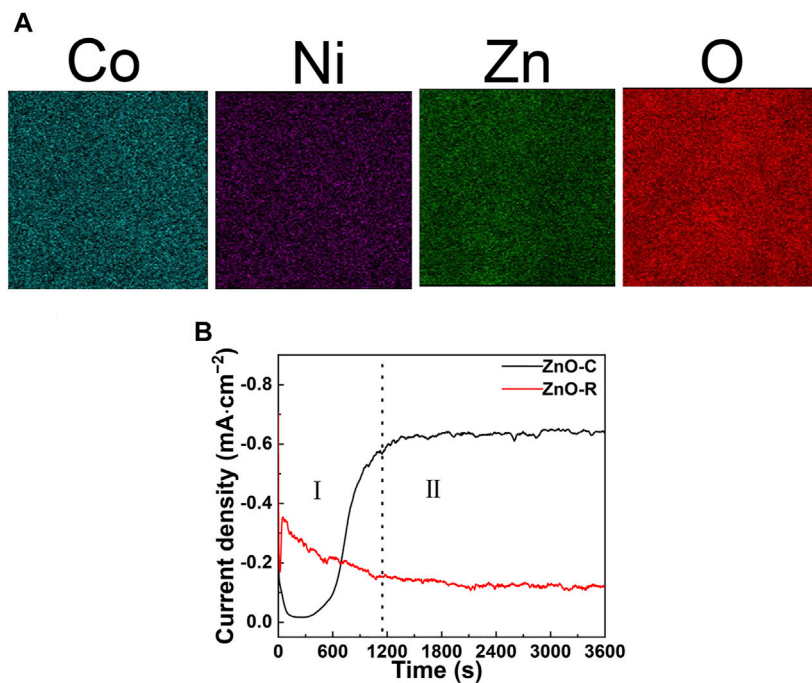


FIGURE 2 | EDS elemental mapping of LDH/ZnO-C (A) and current density–time response during the electrodeposition of ZnO films (B).

illumination with a 300-W xenon lamp (CEL-HXF300, Beijing Zhongjiaojinyuan Technology Co. Ltd., China) as the light source. The photocurrent was obtained by measuring the

coupling current between 304SS and the FTO electrode deposited with different composite films. As a comparison, the OCP and current density of the samples were also measured when

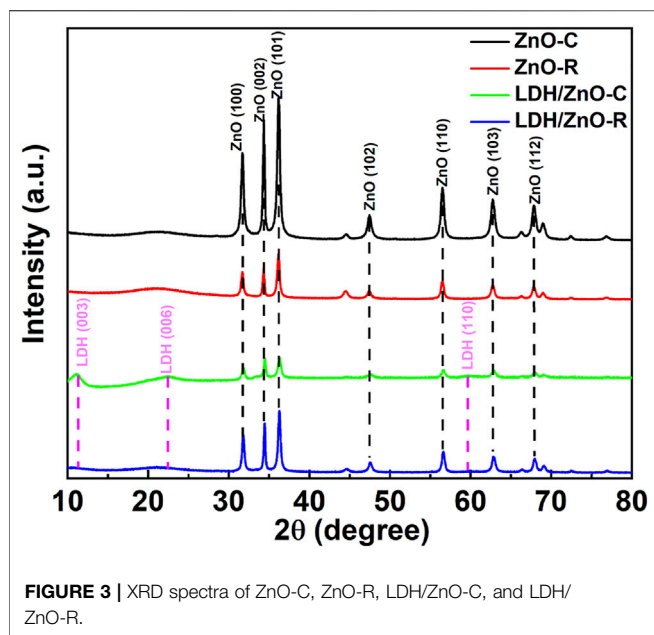


FIGURE 3 | XRD spectra of ZnO-C, ZnO-R, LDH/ZnO-C, and LDH/ZnO-R.

hole scavengers (0.1 M Na_2SO_3 mixed with 0.2 M NaOH) were added in the electrolyte.

The potentiodynamic polarization curves were plotted from -50 to 150 mV relative to OCP, with the scan rate of $1 \text{ mV}\cdot\text{s}^{-1}$. Electrochemical impedance spectroscopy (EIS) was carried out with the AC amplitude of 5 mV and frequency ranging from 0.01 Hz to 100 kHz . The Mott–Schottky plots were conducted in the dark environment with the frequency and AC magnitude of $1,000 \text{ Hz}$ and 10 mV , respectively.

RESULTS AND DISCUSSION

Morphologies and Chemical Compositions

Figure 1 shows the morphologies of ZnO and CoNi-LDH/ZnO deposited on the surface of 304SS. In Figure 1A, the diameter of the ZnO nanocluster varied from 200 to 300 nm , with dense and rough structures, while ZnO, as shown in Figure 1B, was a hexagonal columnar nanorod with a diameter of about 150 nm and a length of about $1 \mu\text{m}$, which was consistent with that in previous studies (Liu et al., 2021). Figure 2B recorded the variation curves of current density during the electrodeposition process of the ZnO nanocluster (denoted as ZnO-C) and ZnO nanorod (denoted as ZnO-R). The current density of ZnO-R was higher in the initial stage (stage I), indicating more surface nucleation, while during the equilibrium stage (stage II), the current density of ZnO-C was almost three times than that of ZnO-R. The larger deposition current represented faster deposition speed, which was the reason that the diameter of ZnO-C was larger than that of ZnO-R. In Figure 1C, the morphology of CoNi-LDH/ZnO-C exhibited foliated structure, which was the typical morphology of LDHs (Nguyen et al., 2017). Because of the overlapped and large deposition amount of LDH nanosheets, ZnO-C was

completely covered by the LDH layer, and the thickness of CoNi-LDH/ZnO-C was $15.7 \pm 2.4 \mu\text{m}$. The EDS elemental distribution of LDH/ZnO-C is shown in Figure 2A. It can be concluded that LDH deposited uniformly on the surface of ZnO-C. Different from the foliated structure of LDH/ZnO-C, the morphology of LDH/ZnO-R was similar to ZnO nanorods, and some LDH nanosheets deposited at the bottom or on the surface of ZnO nanorods, which was consistent with the literature (Shao et al., 2014). The thickness of CoNi-LDH/ZnO-R was $8.3 \pm 1.2 \mu\text{m}$, which was less than that of CoNi-LDH/ZnO-C. The difference of morphologies could be related to the difference of deposition time and electrical conductivity of ZnO films.

The XRD spectra of ZnO-C, ZnO-R, LDH/ZnO-C, and LDH/ZnO-R are presented in Figure 3. It can be seen from the spectra that the diffraction peaks of ZnO-R and ZnO-C were both narrow and clear, indicating that the crystallinity of ZnO was excellent. The peaks were consistent with a standard diffraction pattern (PDF#89-1397). In detail, the peaks at 31.6° , 34.3° , and 36.1° represented the crystal planes of (100), (002), and (101), respectively. Therefore, the crystal structure of ZnO was hexagonal wurtzite (Skompska and Zarębska, 2014). After the deposition of LDH nanosheets, the intensity of the related diffraction peaks of ZnO was weakened in the spectra of LDH/ZnO-C and LDH/ZnO-R, which could be ascribed to the physical shielding function of LDH deposited on ZnO. Simultaneously, in the spectrum of LDH/ZnO-C, the emerging peaks of LDH at 11.3° , 22.7° , and 59.9° belonged to (003), (006), and (110) planes of the hydroxalite-like phase, respectively. Among them, the (003) plane is a typical peak for hydroxalite-like materials. Therefore, it can be concluded that LDH was successfully deposited on ZnO-C. In addition, the characteristic peak of LDH was not obvious in the spectrum of LDH/ZnO-R, which could be due to the low deposition amount of LDH.

In order to analyze the surface components and valences of the elements of the LDH/ZnO-C film, the XPS analysis is depicted in Figure 4. In Figure 4A, the full survey scan indicated the main elements of the LDH/ZnO-C film, such as C, O, Co, Ni, and Zn. The peak of the C element was probably ascribed to the doping of CO_3^{2-} originated from CO_2 in the air. The high-resolution spectra of Zn 2p, O 1s, Ni 2p, and Co 2p are presented in Figures 4B–E. In the spectrum of Zn 2p (Figure 4B), the peaks at $1,021 \text{ eV}$ and $1,045 \text{ eV}$ confirmed the presence of Zn–O in the LDH/ZnO-C composite. Specifically, in Figure 4C (O 1s spectrum), the peak at 530.6 eV belonged to Zn–O, and the O_2 (531.1 eV) and O_3 (531.6 eV) peaks represented Ni–O and Co–O, respectively; the O_4 peak at 532.1 eV was ascribed to the –OH group in the metal hydroxide; the O_5 (532.8 eV) was attributed to adsorbed water. In Figure 4D, the double-spin orbit peak and corresponding satellite peaks can be observed in the spectrum for Ni 2p. The peaks located at 856.4 and 873.8 eV corresponded to $2p_{3/2}$ and $2p_{1/2}$ of Ni, respectively. Correspondingly, the satellite peaks appeared at 862.0 and 879.6 eV . Hence, Ni with a chemical state of +2 existed as a form of Ni–O. In the spectrum of Co 2p (Figure 4E), the atomic orbitals of Co $2p_{3/2}$ and Co $2p_{1/2}$ can be confirmed by the peaks at 781.0 and 796.6 eV , respectively. Four peaks appeared in the fitting curve in Figure 4E. Co $2p_{3/2}$

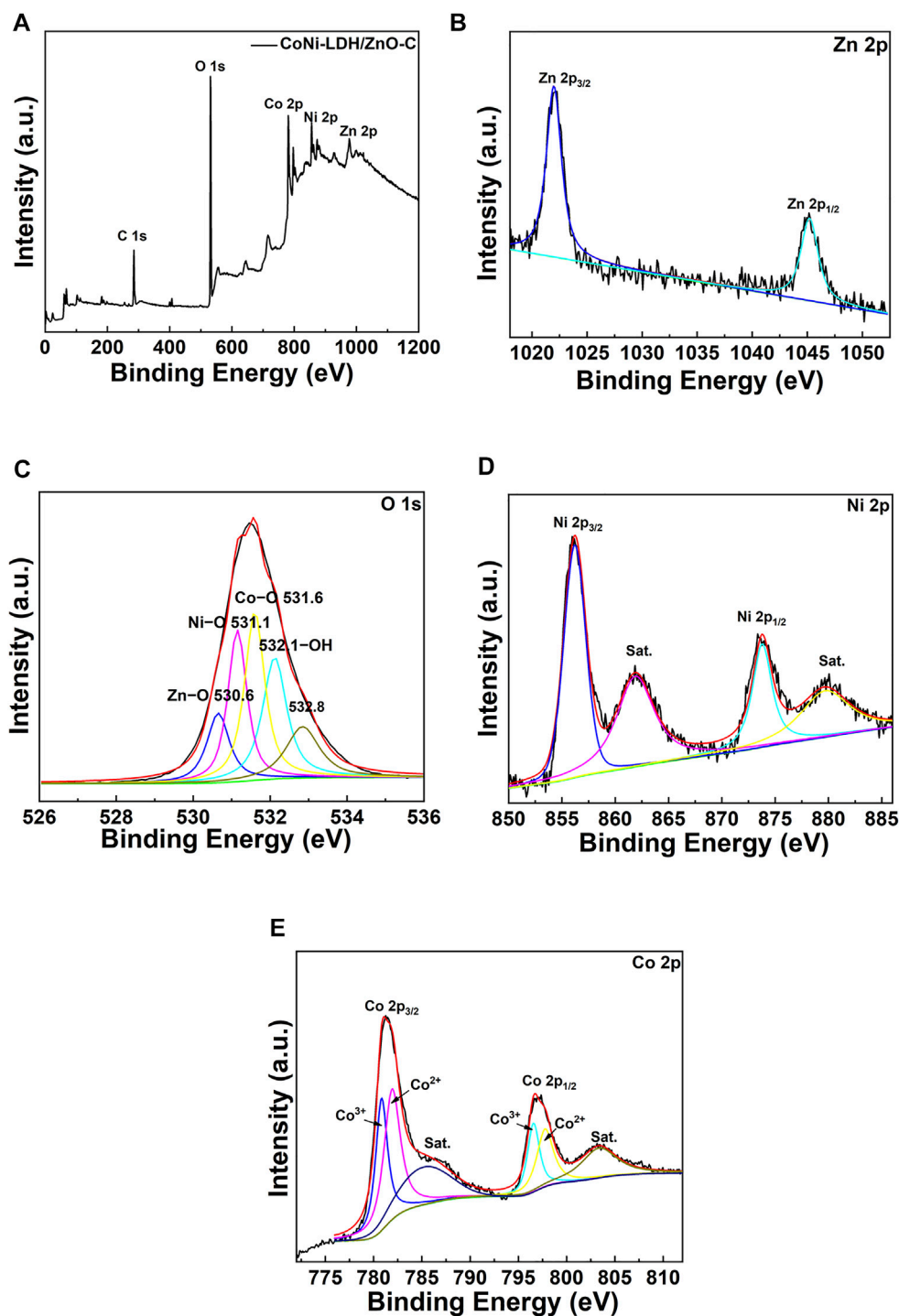


FIGURE 4 | XPS spectra of the LDH/ZnO-C composite: **(A)** the full survey scan, **(B)** Zn 2p, **(C)** O 1s, **(D)** Ni 2p, and **(E)** Co 2p.

peak split to the double peaks at 780.8 and 782.2 eV; at the same time, Co 2p_{1/2} peak split to the double peaks at 796.0 and 797.5 eV. The peaks at 780.8 and 796.0 eV were caused by the presence of Co³⁺, while the peaks at 782.2 and 797.5 eV were referred to the presence of Co²⁺. The results were similar to those of the previous investigation about the Co 2p atomic orbital (Bai

et al., 2019), indicating that the valence of Co in the film was mainly Co²⁺ and Co³⁺.

Optical Absorption Properties

As presented in **Figure 5**, the UV-Vis diffuse reflectance spectra were used to analyze the absorption performance of the samples.

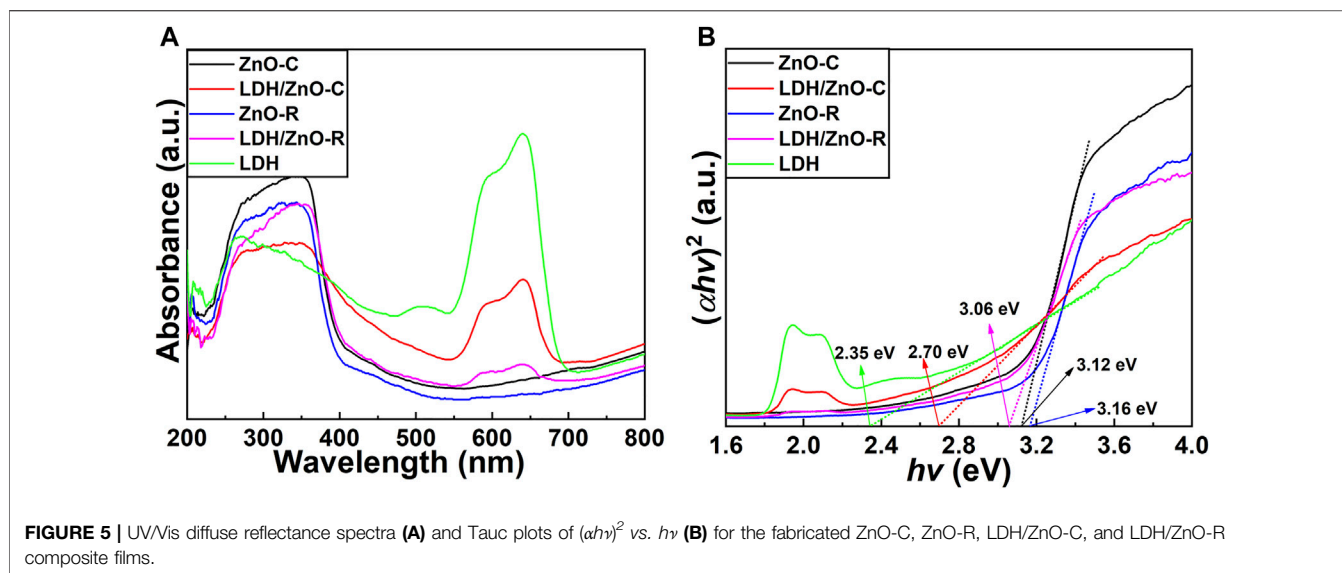


FIGURE 5 | UV/Vis diffuse reflectance spectra (A) and Tauc plots of $(\alpha h\nu)^2$ vs. $h\nu$ (B) for the fabricated ZnO-C, ZnO-R, LDH/ZnO-C, and LDH/ZnO-R composite films.

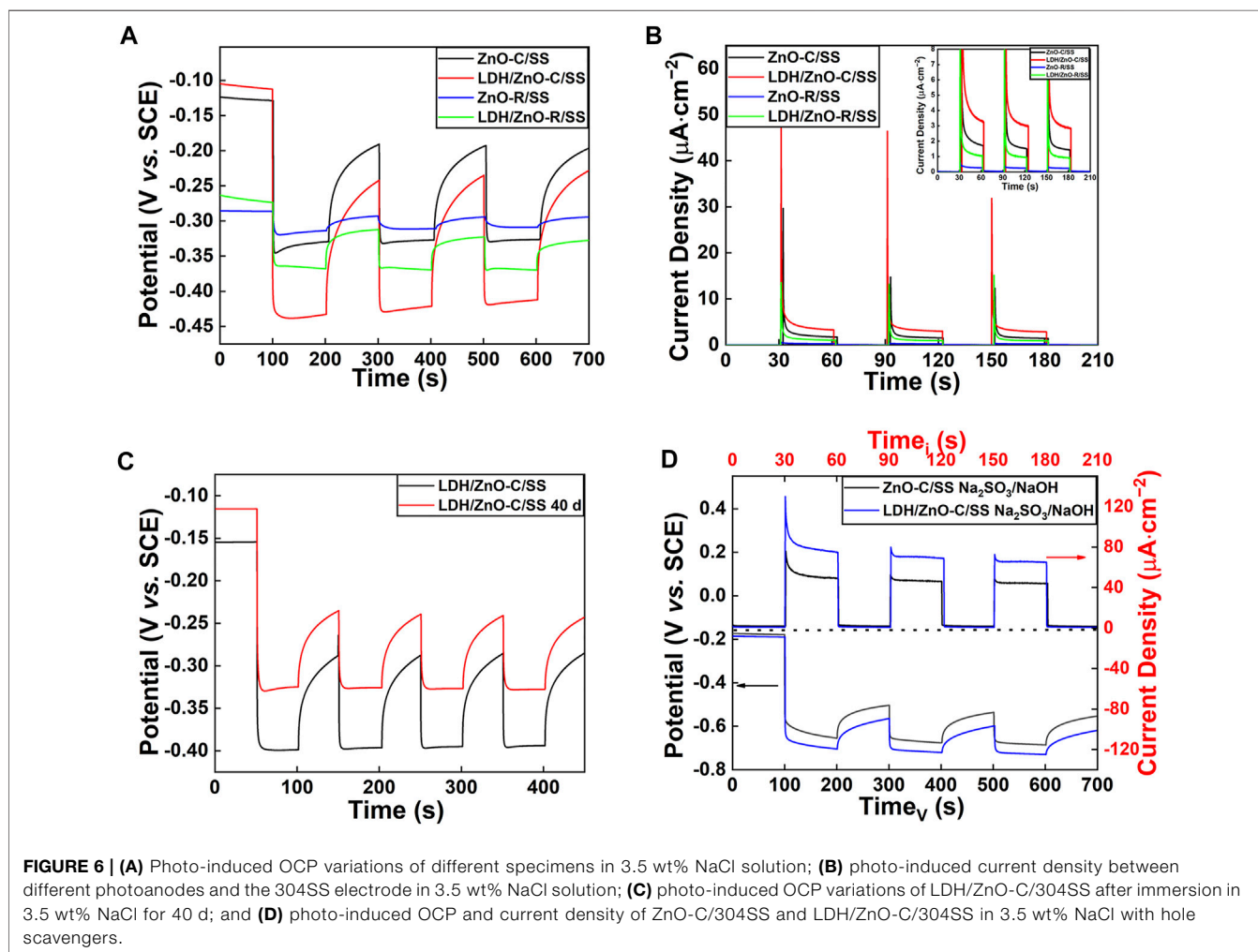


FIGURE 6 | (A) Photo-induced OCP variations of different specimens in 3.5 wt% NaCl solution; (B) photo-induced current density between different photoanodes and the 304SS electrode in 3.5 wt% NaCl solution; (C) photo-induced OCP variations of LDH/ZnO-C/304SS after immersion in 3.5 wt% NaCl for 40 d; and (D) photo-induced OCP and current density of ZnO-C/304SS and LDH/ZnO-C/304SS in 3.5 wt% NaCl with hole scavengers.

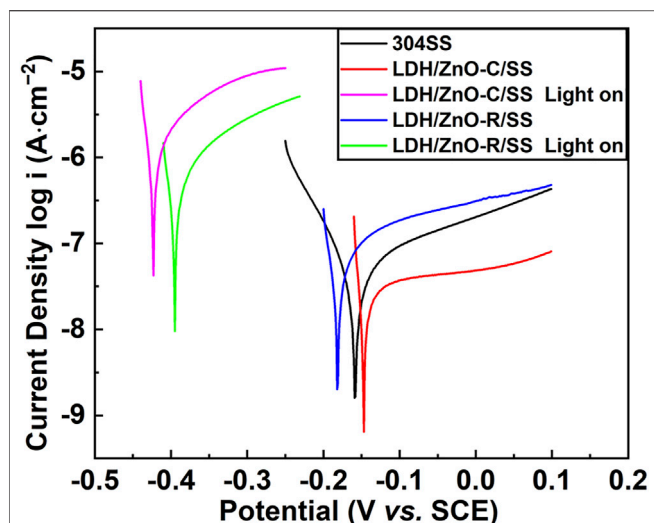


FIGURE 7 | Polarization curves of different specimens under dark or illumination conditions.

In **Figure 5A**, ZnO showed absorbance capacity from 250 to 400 nm owing to the intrinsic property of ZnO (Segets et al., 2009). The edge of the absorption band was approximately 400 nm, indicating that the absorption was mainly in the ultraviolet region. In addition, the absorbance of ZnO-C was higher than that of ZnO-R, which could be attributed to the coarse surface of the nanoclusters and larger active surface of ZnO-C. In the spectra of LDH/ZnO, an obvious absorption band could be observed in the range of 550–650 nm. The emergence of new peaks in visible region indicated that the deposition of LDH broadened the absorption range of the composite film. Moreover, both the absorption peaks of LDH/ZnO-C and LDH/ZnO-R showed red shift. Although the absorbance of LDH/ZnO-C weakened in the ultraviolet region due to the physical shielding effect of LDH, the absorbance was enhanced in the visible region.

In order to obtain the band gap (E_g) of the prepared sample, UV/Vis diffuse reflectance spectra were transferred to the Tauc plot method by **Eq. 1** (Tauc et al., 1966):

$$\alpha h\nu = A(h\nu - E_g)^\eta, \quad (1)$$

where α , h , ν , A , and η represent the absorption coefficient, Planck's constant, light frequency, constant, and transition characteristics of semiconductor, respectively. As the electron in ZnO is excited directly from VB to CB, η is determined as 0.5. The Tauc plots of $(\alpha h\nu)^2$ vs. $h\nu$ are exhibited in **Figure 5B**. The band gap (E_g) was determined by the intersection of the slope of the curve and the X axis. It could be derived that E_g of ZnO-C, ZnO-R, and LDH were 3.12, 3.16, and 2.35 eV, respectively. Moreover, the E_g of LDH/ZnO-C was 2.70 eV, lower than that of LDH/ZnO-R 3.06 eV. The lower E_g was beneficial for the absorption of light, indicating that the LDH/ZnO-C film might exhibit improved photoelectrochemical activity.

In addition, the valence band (E_{VB}) and the conduction band (E_{CB}) positions can be determined by **Eqs 2, 3** (Zhao et al., 2018):

$$E_{VB} = X - E^C + 0.5E_g \quad (2)$$

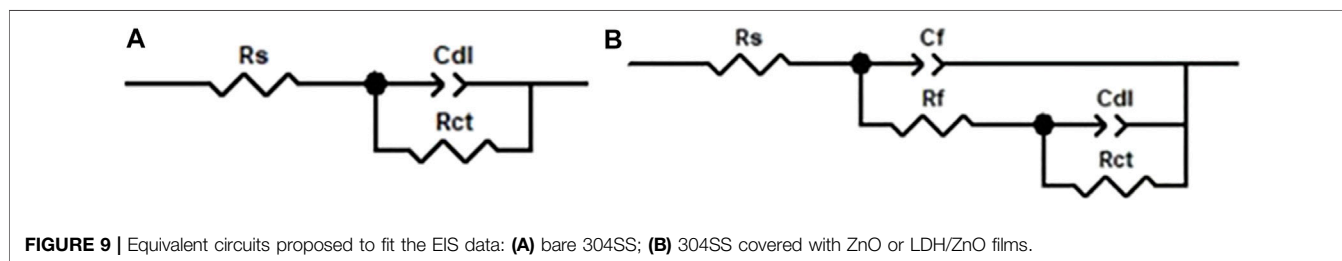
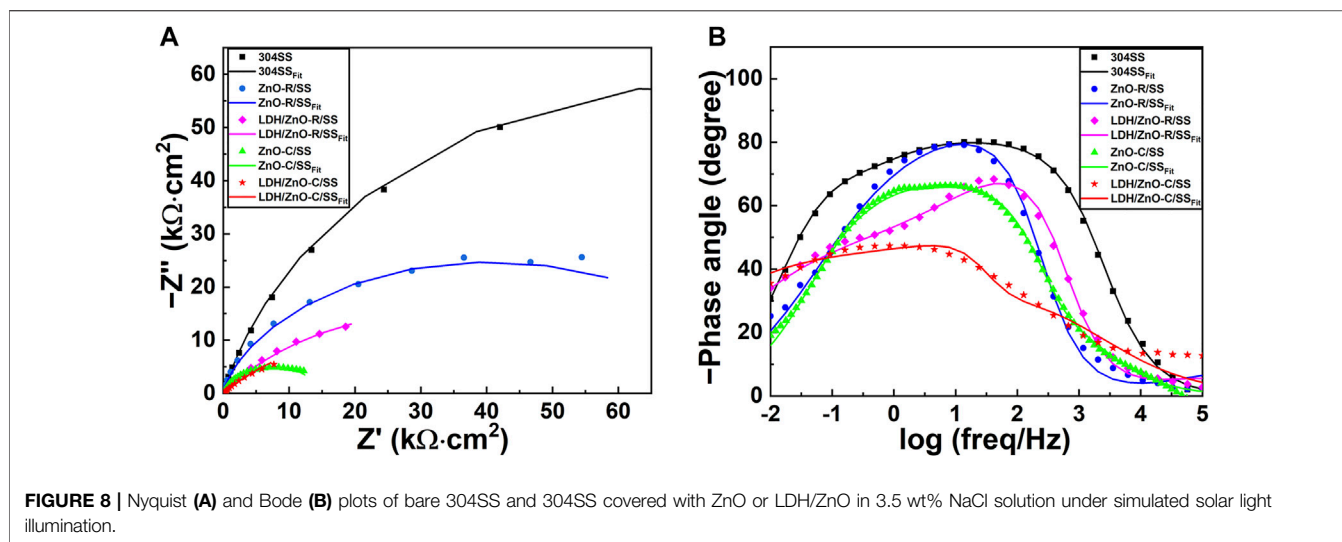
$$E_{CB} = X - E^C - 0.5E_g. \quad (3)$$

where E^C is about 4.5 eV, which represents the energy of the free electrons on the hydrogen scale; E_g and X represent the band gap energy and absolute electronegativity, respectively. For ZnO-C and CoNi-LDH, X values were 5.79 and 4.33 eV, respectively. Therefore, E_{CB} and E_{VB} of ZnO-C were determined to be -0.27 and 2.85 eV vs. SCE (equivalent to -0.03 and 3.09 eV vs. NHE), respectively. Similarly, for CoNi-LDH, E_{CB} and E_{VB} were calculated to be -1.35 and 1.00 eV vs. SCE (equivalent to -1.11 and 1.24 eV vs. NHE).

Photocathodic Protection Performances

To investigate the photocathodic protection performance of ZnO and LDH/ZnO films, the variations of OCP and current density were measured under different conditions without applying any bias voltage, as shown in **Figure 6**. Without the hole scavengers, the open-circuit potential of the 304SS electrode deposited with ZnO or LDH/ZnO presented significant negative shift under illumination condition. Moreover, the deposition of LDH promoted the negative shift of OCP (**Figure 6A**), which could be attributed to the enhanced light absorption and the capture of holes of LDH. Simultaneously, the potential of the 304SS electrode deposited with LDH/ZnO-R decreased to -360 mV, while the electrode deposited with LDH/ZnO-C decreased to -430 mV. The larger negative shift of the photo-induced OCP indicated that the LDH/ZnO-C film exhibited a better cathodic protection effect. This was consistent with the result of the photocurrent density experiment. As shown in **Figure 6B**, the LDH/ZnO-C film showed the maximum transient photocurrent ($48 \mu\text{A cm}^{-2}$) and steady photocurrent ($4.0 \mu\text{A cm}^{-2}$) without the hole scavengers. Combined with the SEM and UV-Vis results, the photocathodic protection performance of large-sized LDH/ZnO-C was better than that of small-sized LDH/ZnO-R because the larger actual surface area can provide more photoelectrochemical active sites. In order to realize the application in the marine environment, the prepared LDH/ZnO-C/304SS sample was immersed in 3.5 wt% NaCl solution for 40 days to study the long-term effect of immersion on the sample. As depicted in **Figure 6C**, the photo-induced potential stabilized at -320 mV after immersion for 40 days. Compared with the newly prepared LDH/ZnO-C/304SS electrode, the photo-induced potential drop decreased, but it could still provide partial protection for the metal. The decrease of the protection performance could be attributed to the local damage of the LDH surface, which resulted from the erosion of chloride ions during long time immersion (**Supplementary Figure S1**).

For comparison, the hole scavengers (0.1 M Na_2SO_3 mixed with 0.2 M NaOH) were added in 3.5 wt% NaCl solution, as shown in **Figure 6D**. With the hole scavengers, the photo-induced OCP dropped and current density increased significantly due to the capture of the holes and the effective separation of electron-hole pairs. Although excellent photocathodic protection performance can be achieved with



the addition of hole scavengers, it is difficult to apply the hole scavengers such as Na_2S or Na_2SO_3 in practical applications. **Supplementary Table S1** shows a comparison of our work with the most recent report. The CoNi-LDH/ZnO-C in our work exhibited competitive photocathodic performance and practical application prospect.

Figure 7 shows the polarization curves of the 304SS electrode with or without the CoNi-LDH/ZnO film under dark or illumination conditions. The calculated electrochemical parameters are listed in **Supplementary Table S2**. Under dark condition, the LDH/ZnO-C/304SS electrode showed positive corrosion potential (-150 mV) and lower current density in the anodic polarization curve than bare 304SS (-170 mV). This could be related to the denser and thicker film of LDH/ZnO-C, which provided a protective film to reduce the contact between the metal and corrosive medium. However, the LDH/ZnO-R/304SS electrode exhibited negative corrosion potential (-180 mV) and higher current density in the anodic polarization curve. This abnormal phenomenon might be caused by the higher temperature during the deposition process of ZnO-R, which had a certain effect on the stainless steel substrate.

Under the illumination condition, the E_{corr} of LDH/ZnO-C/304SS and LDH/ZnO-R/304SS electrodes decreased to -420 mV and -390 mV, respectively. This was consistent with the trend observed in photo-induced potential tests (**Figure 6A**). This result revealed that the photoelectric conversion efficiency of

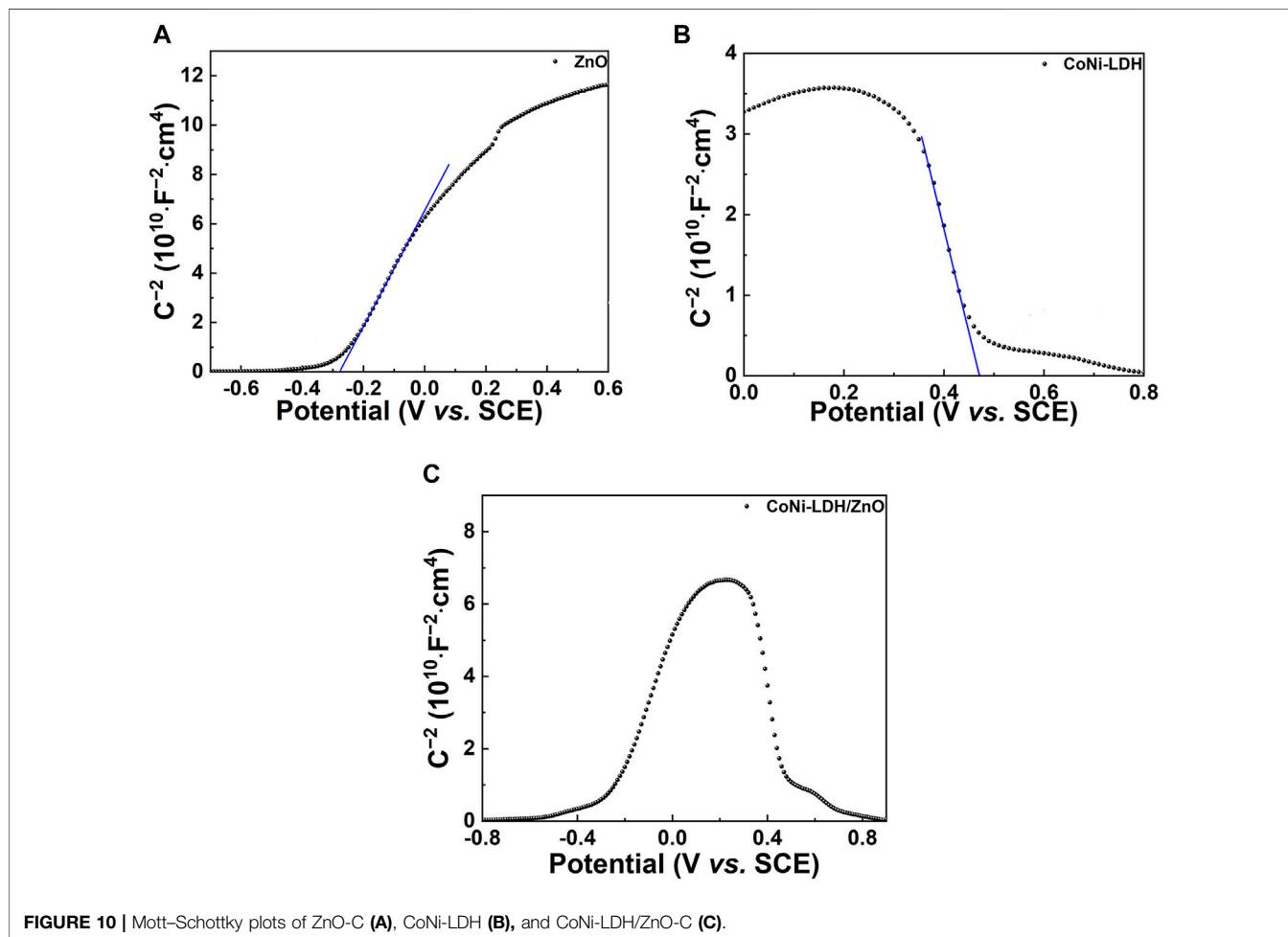
the LDH/ZnO-C film was higher than that of the LDH/ZnO-R film. Moreover, LDH/ZnO-C/304SS had the largest I_{corr} ($3.61 \mu\text{A cm}^{-2}$), indicating that LDH/ZnO-C can produce more photoelectrons than LDH/ZnO-R. It could be deduced that the LDH/ZnO-C film had more effective physical blocking effect under dark conditions and better photocathodic protection performance under illumination conditions. Therefore, the LDH/ZnO-C film had more comprehensive anticorrosion protection for metals.

The EIS tests were performed in 3.5 wt% NaCl solution under simulated solar illumination conditions, as shown in **Figure 8**. In order to fit the EIS data, the equivalent circuits are shown in **Figure 9**, where R_s , R_{ct} , C_{dl} , R_f , and C_f represent the solution resistance, charge transfer resistance, double layer capacitance, film resistance, and film capacitance, respectively. Because the response of interface capacitance is not ideal, the constant phase angle element is used instead of standard capacitance.

The fitting results of the equivalent circuit are shown in **Table 1**. Compared with LDH/ZnO-R/304SS, LDH/ZnO-C/304SS had a smaller R_{ct} value, indicating that the LDH/ZnO-C film had a faster charge transfer rate, which was more favorable for the separation and transmission of photo-generated carriers. Moreover, LDH/ZnO-C/304SS had a higher R_f value, illustrating that the LDH/ZnO-C film had a better physical blocking effect. The high R_f value could be attributed to the deposition and stacking of LDH on the denser and thicker ZnO-C film. Moreover, the deposition of

TABLE 1 | Fitting results of EIS data for different specimens in 3.5 wt% NaCl solution under simulated solar light illumination (the error is presented).

Sample	R_s ($\Omega\cdot\text{cm}^2$)	C_f (μF)	R_f ($\Omega\cdot\text{cm}^2$)	C_{dl} (μF)	R_{ct} ($\Omega\cdot\text{cm}^2$)
304SS	3.90 (1.8%)	—	—	46.49 (1.5%)	134,750 (3.5%)
ZnO-R/304SS	21.76 (10.5%)	27.52 (3.4%)	15.95 (15.9%)	16.98 (2.7%)	89,544 (6.6%)
LDH/ZnO-R/304SS	12.79 (3.0%)	135.63 (1.4%)	6.95 (9.0%)	12.83 (2.5%)	68,483 (9.2%)
ZnO-C/304SS	11.92 (0.5%)	170.96 (0.6%)	24.82 (7.6%)	12.30 (5.1%)	15,205 (1.0%)
LDH/ZnO-C/304SS	26.78 (2.9%)	382.82 (2.2%)	386 (18.7%)	12.07 (16.0%)	54,512 (18.6%)



the visible light responsive CoNi-LDH could provide more catalytic active sites and achieve higher photoelectric conversion efficiency.

Photocathodic Protection Mechanism Analysis

Figure 10 shows the Mott-Scottky (MS) curves of the prepared material. The slope of the MS curve corresponding to ZnO was positive (Figure 10A), indicating that the prepared ZnO was an *n*-type semiconductor while the slope was negative for CoNi-LDH in Figure 10B, which confirmed that CoNi-LDH was a *p*-type semiconductor. As for the CoNi-LDH/ZnO-C film (Figure 10C),

the slope of the MS curve was positive as the potential was lower than 0.2 V, but the slope changed to be negative when the potential became larger than 0.2 V. In summary, the trend of the slope presented an inverted “V” shape from positive to negative, indicating that the *p*-*n* heterojunction was formed successfully by the composition of ZnO-C and CoNi-LDH. The formation of the heterojunction made the photoelectrons and holes move toward the opposite direction, which suppressed the recombination of photo-generated carriers and enhanced the efficiency of photoelectric conversion.

Figure 11 shows the anticorrosion mechanism of the CoNi-LDH/ZnO film. Under simulated solar light illumination, the electrons in the VB of ZnO and CoNi-LDH were excited and jumped to their CB, leaving holes in the VB. ZnO, as *n*-type

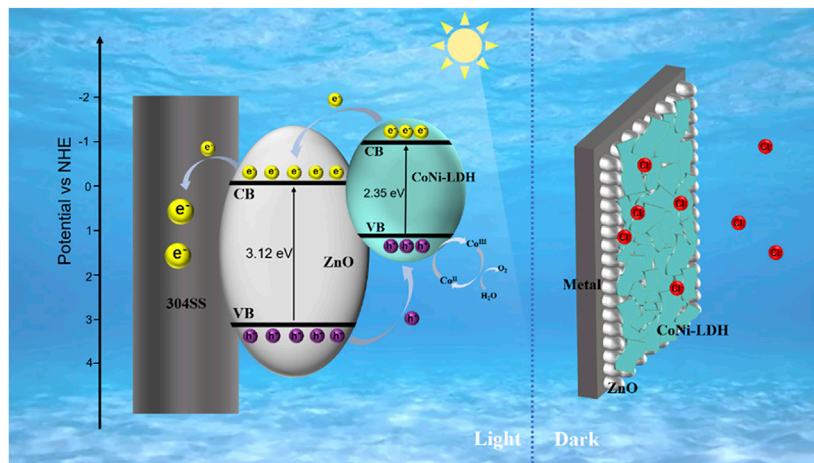


FIGURE 11 | Schematic illustration of the anticorrosion mechanism of the CoNi-LDH/ZnO-C film.

semiconductor, formed *p-n* heterojunction at the interface with CoNi-LDH, which had *p*-type semiconductor properties. Due to the interfacial potential difference, the photoelectrons were transferred from the CB of CoNi-LDH to the CB of ZnO, and the photo-generated holes in the VB of ZnO were transferred to the VB of CoNi-LDH. The photoelectrons accumulated in the CB of ZnO were continuously transferred and accumulated on the surface of the metal, polarizing its potential to a more negative value, thus achieving effective photocathodic protection.

CoNi-LDH had a narrower band gap than ZnO, which enhanced the absorption of visible light. Moreover, CoNi-LDH, as a co-catalyst (Shao et al., 2014), provided abundant active sites for photocatalysis. In the process of charge transfer, Co (II) was oxidized to Co (III), and the photo-generated holes were captured and consumed. Furthermore, Co (III) reacted with water molecules and could be reduced to Co (II) again. Therefore, the cycle of the redox couples Co (II)/Co (III) inhibited the recombination of electron hole pairs (Fan et al., 2020) and improved the photoelectric conversion efficiency of the composite film. In addition, ZnO-C deposited with a thick LDH layer had a good blocking effect and excellent ability to trap chlorine ions, forming a physical barrier on the metal surface in a dark state. Therefore, the CoNi-LDH/ZnO film can effectively protect the metal from corrosion under light or dark conditions.

CONCLUSION

The CoNi-LDH/ZnO nanocluster film exhibits good photocathodic protection and physical isolation performance in NaCl solution, which has the potential of application in the marine environment. The photocathodic protection performance of the CoNi-LDH/ZnO nanocluster film was better than that of the ZnO nanocluster, which was attributed to the visible light response of CoNi-LDH, the formation of *p-n* heterojunction at the interface, and the following depletion of holes by CoNi-LDH. Compared with the traditional CoNi-LDH/ZnO nanorods, CoNi-LDH/ZnO nanoclusters have a higher electron transfer rate and better ability

to capture holes, which was beneficial for the separation of photo-generated carriers and the application in the marine environment without extra hole scavengers. In addition, the dense ZnO nanoclusters and the thick LDH layers could provide superior physical blocking ability to isolate corrosive media under dark condition.

DATA AVAILABILITY STATEMENT

The original contributions presented in the study are included in the article/**Supplementary Material**, further inquiries can be directed to the corresponding authors.

AUTHOR CONTRIBUTIONS

XZ: Conceptualization data curation, formal analysis, investigation, methodology, writing—original draft, and writing—review and editing. YW: Supervision, conceptualization, formal analysis, investigation, resources, methodology, project administration, and writing—review and editing. DZ: Methodology, conceptualization, Instrument provision, and resources. ZT: Supervision, formal analysis, project administration, and writing—review and editing.

FUNDING

This work was supported by the National Natural Science Foundation of China (No. 42090044) and the Senior User Project of RV KEXUE (No. KEXUE 2018G17).

SUPPLEMENTARY MATERIAL

The Supplementary Material for this article can be found online at: <https://www.frontiersin.org/articles/10.3389/fmats.2022.904555/full#supplementary-material>

REFERENCES

- Bai, S., Li, Q., Han, J., Yang, X., Shu, X., Sun, J., et al. (2019). Photoanode of LDH Catalyst Decorated Semiconductor Heterojunction of BiVO₄/CdS to Enhance PEC Water Splitting Efficiency. *Int. J. Hydrog. Energy* 44 (45), 24642–24652. doi:10.1016/j.ijhydene.2019.07.214
- Bu, Y., and Ao, J.-P. (2017). A Review on Photoelectrochemical Cathodic Protection Semiconductor Thin Films for Metals. *Green Energy Environ.* 2 (4), 331–362. doi:10.1016/j.gee.2017.02.003
- Cao, Y., Zheng, D., Zhang, F., Pan, J., and Lin, C. (2022). Layered Double Hydroxide (LDH) for Multi-Functionalized Corrosion Protection of Metals: A Review. *J. Mater. Sci. Technol.* 102, 232–263. doi:10.1016/j.jmst.2021.05.078
- Chen, R., Xu, Y., Xie, X., Li, C., Zhu, W., Xiang, Q., et al. (2021). Synthesis of TiO₂ Nanotubes/Nickel-Gallium Layered Double Hydroxide Heterostructure for Highly-Efficient Photocathodic Anticorrosion of 304 Stainless Steel. *Surf. Coatings Technol.* 424, 127641. doi:10.1016/j.surfcoat.2021.127641
- Ding, D., Hou, Q., Su, Y., Li, Q., Liu, L., Jing, J., et al. (2019). g-C₃N₄/TiO₂ Hybrid Film on the Metal Surface, a Cheap and Efficient Sunlight Active Photoelectrochemical Anticorrosion Coating. *J. Mater. Sci. Mater. Electron* 30 (13), 12710–12717. doi:10.1007/s10854-019-01635-z
- Fan, L., Zhang, X., Zhang, C., Li, J., Wu, C., Chu, Y., et al. (2020). A Highly Efficient α -Fe₂O₃/NiFe(OH)_x Photoelectrode for Photocathodic Protection of 304 Stainless Steel under Visible Light. *Surf. Coatings Technol.* 403, 126407. doi:10.1016/j.surfcoat.2020.126407
- Guo, J., Yang, X., Bai, S., Xiang, X., Luo, R., He, J., et al. (2019). Effect of Mo Doping and NiFe-LDH Cocatalyst on PEC Water Oxidation Efficiency. *J. Colloid Interface Sci.* 540, 9–19. doi:10.1016/j.jcis.2018.12.069
- He, G., and Wang, K. (2011). The Super Hydrophobicity of ZnO Nanorods Fabricated by Electrochemical Deposition Method. *Appl. Surf. Sci.* 257 (15), 6590–6594. doi:10.1016/j.apsusc.2011.02.083
- Jabbar, A., Yasin, G., Khan, W. Q., Anwar, M. Y., Korai, R. M., Nizam, M. N., et al. (2017). Electrochemical Deposition of Nickel Graphene Composite Coatings: Effect of Deposition Temperature on its Surface Morphology and Corrosion Resistance. *RSC Adv.* 7 (49), 31100–31109. doi:10.1039/c6ra28755g
- Jing, J., Chen, Z., Feng, C., Sun, M., and Hou, J. (2021). Transforming G-C₃N₄ from Amphoteric to N-Type Semiconductor: The Important Role of P/n Type on Photoelectrochemical Cathodic Protection. *J. Alloys Compd.* 851, 156820. doi:10.1016/j.jallcom.2020.156820
- Jing, J. P., Chen, Z. Y., and Bu, Y. Y. (2015). Visible Light Induced Photoelectrochemical Cathodic Protection for 304 SS by In₂S₃-Sensitized ZnO Nanorod Array. *Int. J. Electrochem. Sci.* 10 (10), 8783–8796.
- Kang, Z., Si, H., Zhang, S., Wu, J., Sun, Y., Liao, Q., et al. (2019). Interface Engineering for Modulation of Charge Carrier Behavior in ZnO Photoelectrochemical Water Splitting. *Adv. Funct. Mat.* 29 (15), 1808032. doi:10.1002/adfm.201808032
- Li, Q., Li, W., and An, M. (2018). Sunlight Induced Photoelectrochemical Anticorrosion Effect of Corrosion Product Layers on Electrogalvanized Steel in Simulated Seawater. *Electrochem. Commun.* 90, 39–42. doi:10.1016/j.elecom.2018.03.010
- Li, Q., Zeng, D., and An, M. (2019). Elevating the Photo-Generated Cathodic Protection of Corrosion Product Layers on Electrogalvanized Steel through Nano-Electrodeposition. *Chem. Phys. Lett.* 722, 1–5. doi:10.1016/j.cpl.2019.02.030
- Lin, Y., and Liu, S. (2021). Robust ZnO Nanowire Photoanodes with Oxygen Vacancies for Efficient Photoelectrochemical Cathodic Protection. *Appl. Surf. Sci.* 566, 150694. doi:10.1016/j.apsusc.2021.150694
- Liu, Y., Zhu, Z., and Cheng, Y. (2020). An In-Depth Study of Photocathodic Protection of SS304 Steel by Electrodeposited Layers of ZnO Nanoparticles. *Surf. Coatings Technol.* 399, 126158. doi:10.1016/j.surfcoat.2020.126158
- Liu, Y., Zhu, Z., Cheng, Y., Wei, B., and Cheng, Y. (2021). Effect of Electrodeposition Temperature on the Thin Films of ZnO Nanoparticles Used for Photocathodic Protection of SS304. *J. Electroanal. Chem.* 881, 114945. doi:10.1016/j.jelechem.2020.114945
- Lu, X., Liu, L., Xie, X., Cui, Y., Oguzie, E. E., and Wang, F. (2020). Synergetic Effect of Graphene and Co(OH)₂ as Cocatalysts of TiO₂ Nanotubes for Enhanced Photogenerated Cathodic Protection. *J. Mater. Sci. Technol.* 37, 55–63. doi:10.1016/j.jmst.2019.07.034
- Nguyen, T., Boudard, M., Carmezim, M. J., and Montemor, M. F. (2017). Layered Ni(OH)₂-Co(OH)₂ Films Prepared by Electrodeposition as Charge Storage Electrodes for Hybrid Supercapacitors. *Sci. Rep.* 7 (1), 39980. doi:10.1038/srep39980
- Qiu, P., Sun, X., Lai, Y., Gao, P., Chen, C., and Ge, L. (2019). N-Doped TiO₂@TiO₂ Visible Light Active Film with Stable and Efficient Photocathodic Protection Performance. *J. Electroanal. Chem.* 844, 91–98. doi:10.1016/j.jelechem.2019.05.020
- Segets, D., Gradl, J., Taylor, R. K., Vassilev, V., and Peukert, W. (2009). Analysis of Optical Absorbance Spectra for the Determination of ZnO Nanoparticle Size Distribution, Solubility, and Surface Energy. *ACS Nano* 3 (7), 1703–1710. doi:10.1021/nn900223b
- Shao, M., Ning, F., Wei, M., Evans, D. G., and Duan, X. (2014). Hierarchical Nanowire Arrays Based on ZnO Core-Layered Double Hydroxide Shell for Largely Enhanced Photoelectrochemical Water Splitting. *Adv. Funct. Mat.* 24 (5), 580–586. doi:10.1002/adfm.201301889
- Skompska, M., and Zarębska, K. (2014). Electrodeposition of ZnO Nanorod Arrays on Transparent Conducting Substrates-A Review. *Electrochimica Acta* 127, 467–488. doi:10.1016/j.electacta.2014.02.049
- Sun, M., Chen, Z., Bu, Y., Yu, J., and Hou, B. (2014). Effect of ZnO on the Corrosion of Zinc, Q235 Carbon Steel and 304 Stainless Steel under White Light Illumination. *Corros. Sci.* 82, 77–84. doi:10.1016/j.corsci.2013.12.022
- Tabish, M., Yasin, G., Anjum, M. J., Malik, M. U., Zhao, J., Yang, Q., et al. (2021). Reviewing the Current Status of Layered Double Hydroxide-Based Smart Nanocontainers for Corrosion Inhibiting Applications. *J. Mater. Res. Technol.* 10, 390–421. doi:10.1016/j.jmrt.2020.12.025
- Tauc, J., Grigorovici, R., and Vancu, A. (1966). Optical Properties and Electronic Structure of Amorphous Germanium. *Phys. Status Solidi B-Basic Solid State Phys.* 15 (2), 627–637. doi:10.1002/pssb.19660150224
- Tedim, J., Bastos, A. C., Kallip, S., Zheludkevich, M. L., and Ferreira, M. G. S. (2016). Corrosion Protection of AA2024-T3 by LDH Conversion Films. Analysis of SVET Results. *Electrochimica Acta* 210, 215–224. doi:10.1016/j.electacta.2016.05.134
- Wang, G., Wang, B., Su, C., Li, D., Zhang, L., Chong, R., et al. (2018a). Enhancing and Stabilizing α -Fe₂O₃ Photoanode towards Neutral Water Oxidation: Introducing a Dual-Functional NiCoAl Layered Double Hydroxide Overlayer. *J. Catal.* 359, 287–295. doi:10.1016/j.jcat.2018.01.011
- Wang, X.-T., Ning, X.-B., Shao, Q., Ge, S.-S., Fei, Z.-Y., Lei, J., et al. (2018b). ZnFeAl-layered Double hydroxides/TiO₂ Composites as Photoanodes for Photocathodic Protection of 304 Stainless Steel. *Sci. Rep.* 8, 4116. doi:10.1038/s41598-018-22572-7
- Wei, N., Lin, Y., Li, Z., Sun, W., Zhang, G., Wang, M., et al. (2020). One-Dimensional Ag₂S/ZnS/ZnO Nanorod Array Films for Photocathodic Protection for 304 Stainless Steel. *J. Mater. Sci. Technol.* 42, 156–162. doi:10.1016/j.jmst.2019.09.035
- Xu, D., Liu, Y., Liu, Y., Chen, F., Zhang, C., and Liu, B. (2021). A Review on Recent Progress in the Development of Photoelectrodes for Photocathodic Protection: Design, Properties, and Prospects. *Mater. Des.* 197, 109235. doi:10.1016/j.matdes.2020.109235
- Xu, H., Liu, W., Cao, L., Su, G., and Duan, R. (2014). Preparation of Porous TiO₂/ZnO Composite Film and its Photocathodic Protection Properties for 304 Stainless Steel. *Appl. Surf. Sci.* 301, 508–514. doi:10.1016/j.apsusc.2014.02.114
- Xuan, X., Li, L., Runze, C., Gang, L., Ying, L., and Fuhui, W. (2018). Long-Term Photoelectrochemical Cathodic Protection by Co(OH)₂-Modified TiO₂ on 304 Stainless Steel in Marine Environment. *J. Electrochem. Soc.* 165 (4), H3154–H3163. doi:10.1149/2.0221804jes
- Yang, Y., Cheng, W., and Cheng, Y. F. (2019). Preparation of Co₃O₄@ZnO Core-Shell Nanocomposites with Intrinsic P-N Junction as High-Performance Photoelectrodes for Photoelectrochemical Cathodic Protection under Visible Light. *Appl. Surf. Sci.* 476, 815–821. doi:10.1016/j.apsusc.2019.01.157
- Yang, Y., and Cheng, Y. F. (2018). One-step Facile Preparation of ZnO Nanorods as High-Performance Photoanodes for Photoelectrochemical Cathodic Protection. *Electrochimica Acta* 276, 311–318. doi:10.1016/j.electacta.2018.04.206
- Yasin, G., Arif, M., Nizam, M. N., Shakeel, M., Khan, M. A., Khan, W. Q., et al. (2018a). Effect of Surfactant Concentration in Electrolyte on the Fabrication and Properties of Nickel-Graphene Nanocomposite Coating Synthesized by

- Electrochemical Co-Deposition. *RSC Adv.* 8 (36), 20039–20047. doi:10.1039/c7ra13651j
- Yasin, G., Arif, M., Shakeel, M., Dun, Y., Zuo, Y., Khan, W. Q., et al. (2018b). Exploring the Nickel-Graphene Nanocomposite Coatings for Superior Corrosion Resistance: Manipulating the Effect of Deposition Current Density on its Morphology, Mechanical Properties, and Erosion-Corrosion Performance. *Adv. Eng. Mat.* 20 (7), 1701166. doi:10.1002/adem.201701166
- Yuan, J., and Tsujikawa, S. (1995). Characterization of Sol-Gel-Derived TiO₂ Coatings and Their Photoeffects on Copper Substrates. *J. Electrochem. Soc.* 142 (10), 3444–3450. doi:10.1149/1.2050002
- Zhao, G., Zhang, D., Huang, Y., Yu, J., Jiang, X., and Jiao, F. (2018). Highly Efficient Degradation of 2-Chlorophenol and Methylene Blue with Rb_{0.27}WO₃/NiFe-CLDH Composites under Visible Light Irradiation. *Adv. Powder Technol.* 29 (10), 2491–2500. doi:10.1016/j.apt.2018.06.029
- Zhou, M.-J., Xu, T., and Hu, J.-M. (2021). Ni-Al Layered Double Hydroxide Films Offering Corrosion Protection under Dark or Illuminated Conditions. *Surf. Coatings Technol.* 421, 127416. doi:10.1016/j.surfcoat.2021.127416
- Zhu, Y., Zhao, X., Li, J., Zhang, H., Chen, S., Han, W., et al. (2018). Surface Modification of Hematite Photoanode by NiFe Layered Double Hydroxide for Boosting Photoelectrocatalytic Water Oxidation. *J. Alloys Compd.* 764, 341–346. doi:10.1016/j.jallcom.2018.06.064
- Conflict of Interest:** The authors declare that the research was conducted in the absence of any commercial or financial relationships that could be construed as a potential conflict of interest.
- Publisher's Note:** All claims expressed in this article are solely those of the authors and do not necessarily represent those of their affiliated organizations, or those of the publisher, the editors, and the reviewers. Any product that may be evaluated in this article, or claim that may be made by its manufacturer, is not guaranteed or endorsed by the publisher.

Copyright © 2022 Zhang, Wang, Zhang and Tao. This is an open-access article distributed under the terms of the Creative Commons Attribution License (CC BY). The use, distribution or reproduction in other forums is permitted, provided the original author(s) and the copyright owner(s) are credited and that the original publication in this journal is cited, in accordance with accepted academic practice. No use, distribution or reproduction is permitted which does not comply with these terms.